Voltage Controlled Nanoparticle Plasmon Resonance Tuning through Anodization

Chatdanai Lumdee[a] and Pieter G. Kik[*,a,b]
[a]CREOL, the College of Optics and Photonics; [b]Physics Department,
University of Central Florida, 4000 Central Florida Blvd, Orlando, FL 32816

ABSTRACT

Frequency control of plasmon resonances is important for optical sensing applications such as Surface Enhanced Raman Spectroscopy. Prior studies that investigated substrate-based control of noble metal nanoparticle plasmon resonances mostly relied on metal substrates with organic or oxide spacer layers that provided a fixed resonance frequency after particle deposition. Here we present a new approach enabling continuous resonance tuning through controlled substrate anodization. Localized Surface Plasmon tuning of single gold nanoparticles on an Al film is observed in single-particle microscopy and spectroscopy experiments. Au nanoparticles (diameter 60 nm) are deposited on 100 nm thick Al films on silicon. Dark field microscopy reveals Au nanoparticles with a dipole moment perpendicular to the aluminum surface. Subsequently an Al_2O_3 film is formed with voltage controlled thickness through anodization of the particle coated sample. Spectroscopy on the same particles before and after various anodization steps reveal a consistent blue shift as the oxide thickness is increased. The observed trends in the scattering peak position are explained as a voltage controlled interaction between the nanoparticles and the substrate. The experimental findings are found to closely match numerical simulations. The effects of particle size variation and spacer layer dielectric functions are investigated numerically. The presented approach could provide a post-fabrication frequency tuning step in a wide range of plasmonic devices, could enable the investigation of the optical response of metal nanostructures in a precisely controlled local environment, and could form the basis of chemically stable frequency optimized sensors.

Keywords: plasmon resonance tuning, gold nanoparticle tuning, voltage controlled tuning, anodization, single particle spectroscopy

1. INTRODUCTION

Surface plasmon resonances in metallic nanoparticles, also referred to as Localized Surface Plasmon Resonance (LSPR) has gained a lot of interest due to its ability in provide a high electric field enhancement, the strong field localization that it can provide, and its high sensitivity to the local dielectric environment. The LSPR shows promise in a variety of applications: Surface Enhanced Raman Spectroscopy (SERS),[1-3] Surface Enhanced Fluorescence,[4-6] Surface Enhanced second harmonic generation,[7,8] plasmon enhanced nonlinear refraction and absorption,[9,10] sensors,[11,12] photovoltaics,[13-15] and metamaterials.[16,17]

The surface plasmon resonance frequency of metal nanostructures is sensitive to various parameters, *e.g.* shape, size, material, and local dielectric environment.[18] Precise control of the LSPR frequency is important to effectively harness and utilize the structure, for example to match an available laser wavelength, or to enable Surface Enhanced Resonance Raman at the desired wavelength matching the molecular resonance.[19,20] LSPR wavelength control has been achieved through several different methods, including shape control,[21-23] particle-particle interactions in few-particle clusters,[24,25] and substrate control.[26,27] Despite this broad range of tuning methods, deviations from the intended resonance wavelength do occur which cannot be easily corrected after sample preparation. To resolve this issue, our work investigates a method for continuous resonance tuning on the same nanostructure based on controlled substrate modification. Gold nanoparticles on an aluminum film were used in the experiment. Anodization of the aluminum film leads to the formation of an aluminum oxide (Al_2O_3) layer with a thickness that can be precisely controlled by choosing the anodization voltage.[28] Since gold is chemically stable, anodization is not expected to significantly change the structure of the Au particle, suggesting that any observed optical changes will be due to the generated changes in the

* kik@creol.ucf.edu, phone 1-407-823-4622

Plasmonics: Metallic Nanostructures and Their Optical Properties X, edited by Mark I. Stockman,
Proc. of SPIE Vol. 8457, 84570T · © 2012 SPIE · CCC code: 0277-786/12/$18 · doi: 10.1117/12.930326

local optical environment. Single particle scattering spectra on gold nanoparticles were probed after several steps of anodization showing a high precision chemically controlled plasmon resonance tuning. Numerical simulations were performed to interpret the experimental results, and simulations estimating the effect of particle size variation and the effect of spacer layer are presented. The presented method could be used for resonance optimization of a wide variety of metallic nanostructures, and enables detailed studies of plasmonic interactions with few-nm wavelength control.

2. EXPERIMENTS

2.1 Experimental method

A 100 nm thick aluminum film was deposited on a 3-inch [100] silicon wafer (resistivity > 1 Ω-cm) by thermal evaporation using an Edwards FL 400 Thermal Evaporator at 12 Å/s deposition rate. The sample was cleaved into ~1 cm^2 pieces before gold nanoparticle deposition. A monodispersed colloidal gold nanoparticle solution with a mean particle diameter of 60 nm was used (BB International, United Kingdom). The size variation of the gold nanoparticles in these colloidal solutions is typically provided in terms of a synthesis tolerance, which is different from the actual particle size variation within a given colloidal solution. The batch-specific size dispersion of the colloid used in these studies was ± 2.6 nm based on the vendor specified size histogram, below the listed tolerance of ± 4.8 nm. This difference is important in judging any observed resonance wavelength and scattering intensity variations, as discussed in more detail below. The aqueous colloid was diluted with ethanol at a ratio 1:125 to a concentration of ~2×10^8 particles/mL. Approximately 4 μL of the diluted colloid was dropped on the cleaved aluminum-coated sample using a high precision pipette. The as-prepared samples and the anodized samples were found to lead to excellent surface wetting with the diluted solution, suggesting that the Au nanoparticles spread out across a large fraction of the sample surface. The drop-coated sample was dried using air flow. The samples were inspected using an Olympus BX-51 reflected light optical microscope equipped with standard dark-field optics. Dark-field microscopy images showed well dispersed individual scatterers with similar brightness, attributed to single Au nanoparticles deposited from the solution.

Scattering spectra of single nanoparticles were obtained using a 50× dark-field objective (Olympus MPlanFl 50× BD, N.A.=0.80). The collected signal was sent through a multimode fiber to a spectrometer (Horiba Jobin-Yvon iHR320 monochromator with Synapse CCD array). The collection area on the sample was ~20 μm^2. For each particle a scattering spectrum $I_{sc}(\lambda)$ was obtained from three measured spectra $I(\lambda)$, namely $I_{NP}(\lambda)$, the signal obtained from a region containing a single nanoparticle, $I_{REF}(\lambda)$,, the signal collected from a nearby region without a nanoparticle, and $I_{IN}(\lambda)$, the lamp spectrum. The scattering spectrum was obtained using the relation $I_{sc}=(I_{NP} - I_{REF})/I_{IN}$. Note that this method assumes that the substrate is an approximately frequency independent scatterer, and consequently any significant variations of the scattering response of the substrate itself could affect the obtained scattering spectra. In the measurements presented here, the collected lamp spectra varied by less than 8% across the wavelength range of interest. The detector dark current was recorded and subtracted from all spectra.

After single particle spectroscopy measurements, the sample was anodized at room temperature in a 3 wt.% ammonium tartrate solution in deionized water (>10 MΩ-cm) with a stainless steel counter electrode. This process is known to produce a dense and smooth amorphous barrier-type Al_2O_3 layer with a thickness controlled by the anodization voltage.[28,29] The process was repeated for 7 anodization voltages between 1.5 V and 12 V, on the same sample, followed by spectroscopic measurements as described above. Dark-field microscopy images revealed that most of the particles stay in the same position after anodization, allowing investigation of gold nanoparticle spectra of the same particle before and after various anodization steps. Reference samples were made that underwent exactly the same anodization steps as the nanoparticle-coated sample. The oxide thickness of the reference samples was measured using a J.A. Woollam variable angle spectroscopic ellipsometer and fitting based on literature values for the Al[30] and Al_2O_3[31] dielectric functions.

2.2 Experimental Observation

Figure 1(a) presents the measured aluminum oxide thickness as a function of an anodization voltage. Note that the lowest measured thickness of 3.6 nm corresponds to the well-known self-limited growth of a native oxide on the Al films. Dark-field microscopy images of gold nanoparticles on the anodized aluminum substrate on thin (3.6 nm) and thick (13 nm) Al_2O_3 layers are shown as insets, revealing ring-shaped scattering patterns. This feature indicates a dipole moment of the

gold nanoparticles to be perpendicular (z-polarized) to the aluminum substrate. The darkfield images of the gold nanoparticles indicate a blue-shift as the oxide thickness increases, with the particle color changing from red to green. Figure 1(b) shows a schematic of the single particle scattering measurement geometry as well as the sample structure.

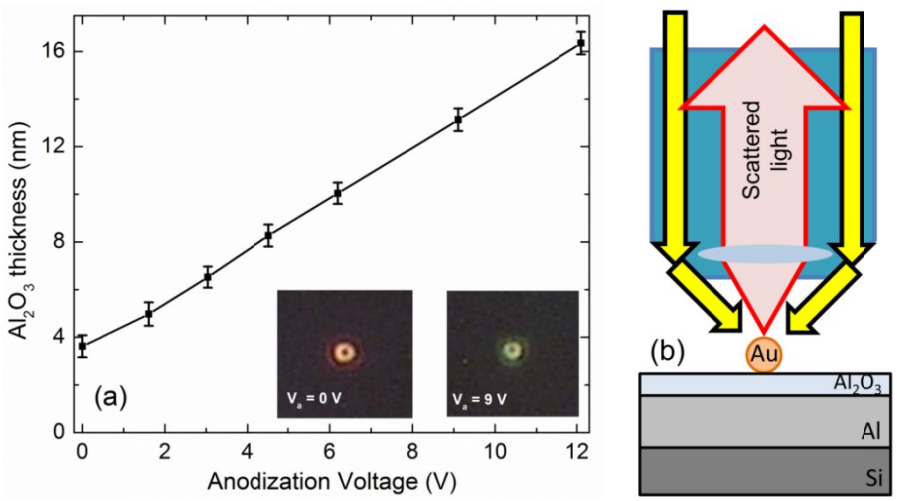

Figure 1. (a) Aluminum oxide thickness as a function of anodization voltage. The insets show dark-field microscopy images of gold nanoparticles at anodization voltages of 0 V and 9 V. (b) Schematic of the measurement and sample geometry.

Figure 2 shows two sets of the single nanoparticle scattering spectra (solid and dashed lines) from the two gold nanoparticles after four anodization steps. The corresponding Al_2O_3 thicknesses are shown in parentheses. A clear blue-shift in the scattering spectra is observed for both particles.

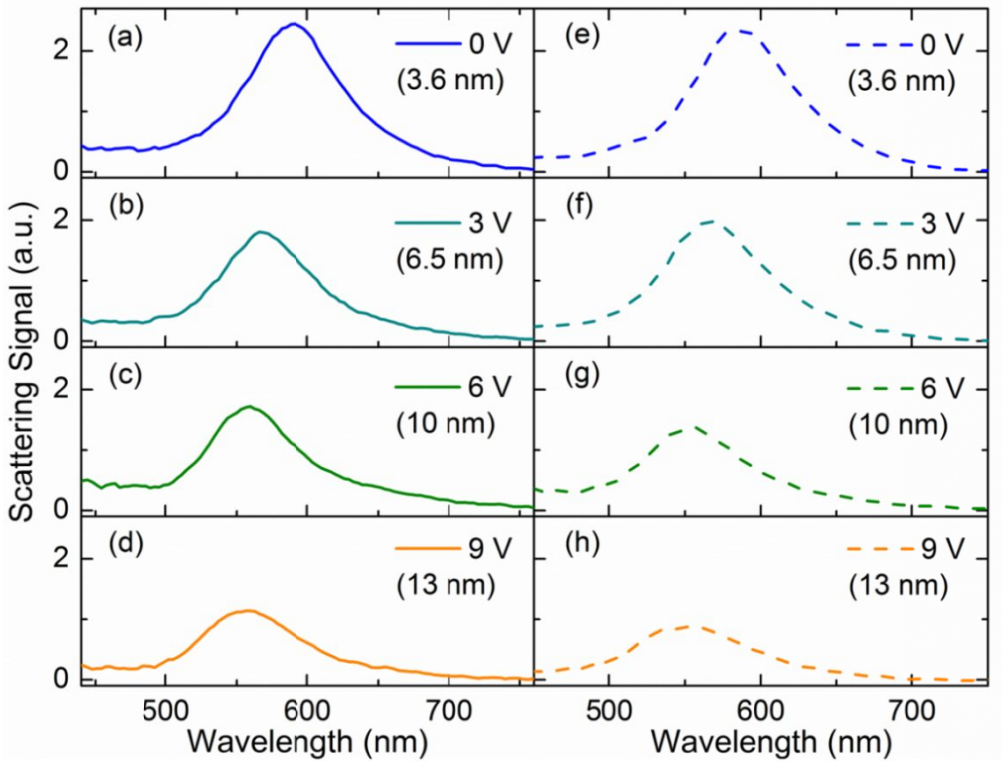

Figure 2. Single particle scattering spectra from two gold nanoparticles after four anodization steps (a)-(d) (solid lines) and (e)-(h) (dashed lines). The corresponding Al_2O_3 thickness after each anodization step is shown in parentheses.

3. NUMERICAL SIMULATION

3.1 Simulation Model and Method

Numerical calculation for single particle scattering spectra were extracted from three-dimensional frequency domain electromagnetic simulations.[32] Figure 3 presents the simulated structure, a 60 nm diameter gold nanoparticle placed on an Al_2O_3 with variable thickness. To avoid scattering of the incident wave at the edge of the sample, periodic boundary conditions were assumed with a lateral unit cell size of 200 × 200 nm^2. Variation of the unit cell size between 180×180 and 220×220 nm^2 was found to lead to scattering wavelength shifts smaller than 3 nm, suggesting that particle-particle coupling through radiation or via excitation of plasmons at the Al-Al_2O_3 interface does not significantly affect the results. Due to the software limitations the silicon substrate was replaced with a SiO_2 (n=1.5) layer. The relatively large Al thickness ensures that the field inside the SiO_2 is small and does not affect the simulation results. Literature data were used for the Al_2O_3,[31] Au,[33] and Al[30] dielectric functions. The structure is illuminated with a plane wave at 53° off the sample normal, corresponding to the numerical aperture (N.A.) of the microscope objective.

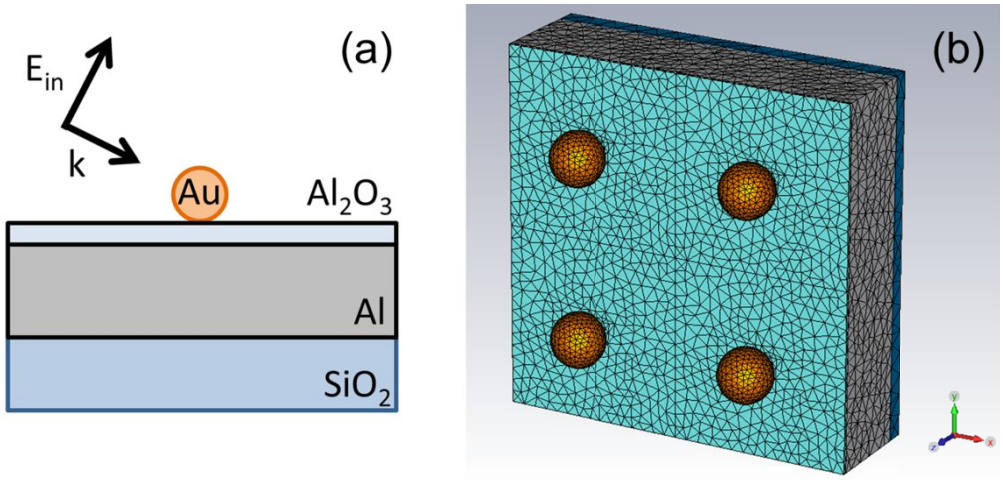

Figure 3. (a) Schematic of the simulated structure and the incident plane wave orientation and polarization, and (b) Numerical simulation model in the software showing the generated tetrahedral mesh with unit cell boundary conditions

The dipole moment of the nanoparticle was calculated using the average electric field inside the nanoparticle at each frequency. Only the z-dipole moment (μ_z) was assumed to contribute to the scattering spectrum, corresponding to the ring-shaped scattering image observed in the experiment. The z-dipole moment was calculated using $\mu_z \sim \chi_{Au} E_{z,ave} V$ with χ_{Au} the gold susceptibility, $E_{z,ave}$ the average electric field in the z-direction in the nanoparticle, and V the nanoparticle volume. The scattered power of the oscillating dipole was assumed to be proportional to $|\mu_z|^2 \omega^4 V^2$ with ω the angular frequency of the dipole oscillation.[34]

4. RESULTS AND DISCUSSIONS

Figure 4 shows the measured peak wavelength obtained from the scattering spectra of four gold nanoparticles at different Al_2O_3 thickness values, as well as the corresponding wavelengths obtained from numerical calculations. The peak wavelength of the gold particles on the aluminum film is seen to be red-shifted relative to the scattering spectrum of a gold nanoparticle in air (~530 nm). This effect can be described as a result of coupling between the gold nanoparticle dipole moment and an image dipole created by free charges in the aluminum film. The agreement between simulations and experimental results strongly suggests that the observed blue-shifting of the scattering spectra is due to a change in the local environment, and not due to changes of e.g. the particle shape, size, or chemical composition. The blue-shifting is attributed to a reduction of the coupling strength between the gold nanoparticle dipole moment and the image dipole in the Al as the particle-Al separation increases. Note that simulated peak wavelengths consistently lie below the experimental observations. This systematic error might originate from a difference between the literature values for the

gold or aluminum dielectric functions and the optical properties of the materials used in the experiment. Alternatively, a chemical residue could be present on the gold nanoparticles or on the substrate related to either the colloidal solution or the anodization chemicals. The simulation results suggest a resonance tuning range in excess of 100 nm could be achieved by placing a gold nanoparticle on an aluminum film with a controlled oxide spacer thickness. This predicted tuning range could not be achieved in the experiment due to the formation of a native Al_2O_3 film on aluminum after exposure to air. The native oxide thickness was measured to be ~3.6 nm on the as-deposited sample.

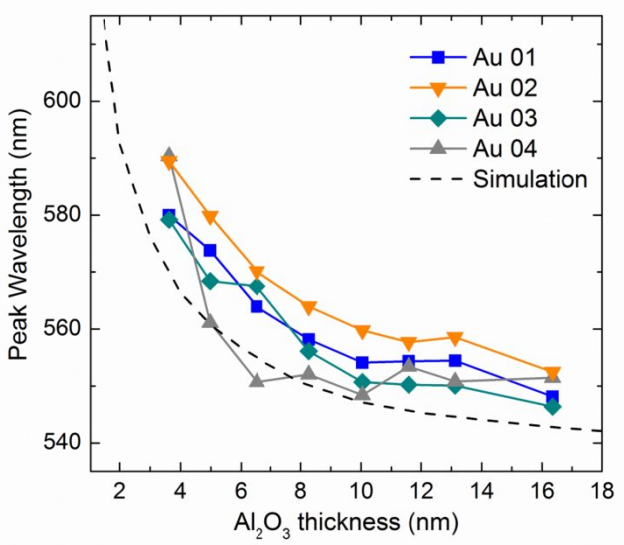

Figure 4. Fitted peak scattering wavelength of four individual gold nanoparticles as a function of Al_2O_3 thickness, as well as the corresponding simulated peak position (dashed line).

Note that the four different gold nanoparticles shown in Fig. 4 exhibit some variation of the peak scattering wavelength at any given anodization voltage. Particles AU01 and AU02 exhibit a virtually identical peak shift, showing only a different offset of ~5.6 nm, possibly due to a difference in nanoparticle size, which is known to affect the particle resonance wavelength as discussed in more detail below. Particle AU03 shows a similar oxide thickness dependence, however at one anodization voltage (6 V) the scattering wavelength deviates from the trend. Random variations such as these might be due to chemical residue on or near the nanoparticle after a given anodization step, resulting in a deviation of the scattering spectrum that could possibly be eliminated by additional cleaning or processing, e.g. after a subsequent anodization step as observed here. Particle AU04 shows a much more sudden drop of the scattering peak wavelength after the first anodization step. This could be the result of an initially locally reduced native oxide thickness for the as-deposited sample, or the presence of a high refractive index or metallic contaminant on or near the particle after colloid deposition.

To investigate the potential effect of particle size variation on the scattering spectra, simulations were done as a function of particle size. The peak wavelengths of single particle scattering spectra for gold nanoparticles with a diameter between 50 and 70 nm on a 4 nm aluminum oxide film were calculated. These thicknesses approximately represent the as-deposited sample with a native oxide thickness as measured in the experiment. Figure 5(a) shows the thus obtained peak scattering wavelength as a function of a gold particle diameter. The scattering peak wavelength exhibits a red shift as the particle diameter increases. Note that the observed wavelength offset of ~5.6 nm between particles AU01 and AU02 in Fig. 4 can be explained by a size difference of only 7 nm. Figure 5(b) shows the particle size distribution histogram provided by the vendor.

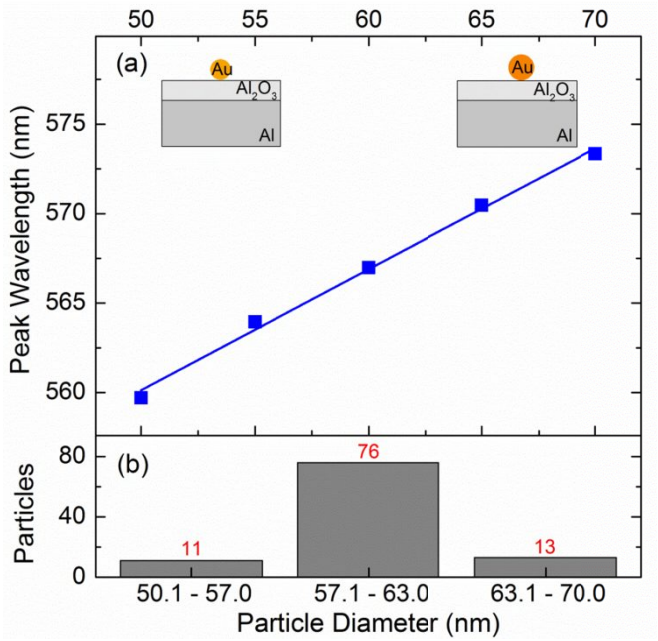

Figure 5. Gold nanoparticle scattering spectra peak wavelength shift as a function of a gold particle diameter for 4 nm and 16 nm Al_2O_3 thicknesses (a), the particle size-distribution histogram (b).

While the wavelength shifts observed in the spectra can be qualitatively understood in terms of a variable interaction between the nanoparticle and its image dipole in the Al film, the presence of the Al_2O_3 layer itself can also affect the resonance wavelength. The influence of the finite polarizability of the Al_2O_3 spacer layer was investigated by repeating the numerical simulations as a function of particle-aluminum separation for a single gold nanoparticle (60 nm diameter) but replacing the Al_2O_3 film with an air gap. Figure 6 shows the simulation results, and for comparison includes the simulation results from Fig. 3. Replacing the Al_2O_3 layer with an air gap is seen to consistently lead to a shorter scattering wavelength. This is expected since metal nanoparticles are known to exhibit increased resonance wavelengths when placed in a high refractive index environment such as Al_2O_3.

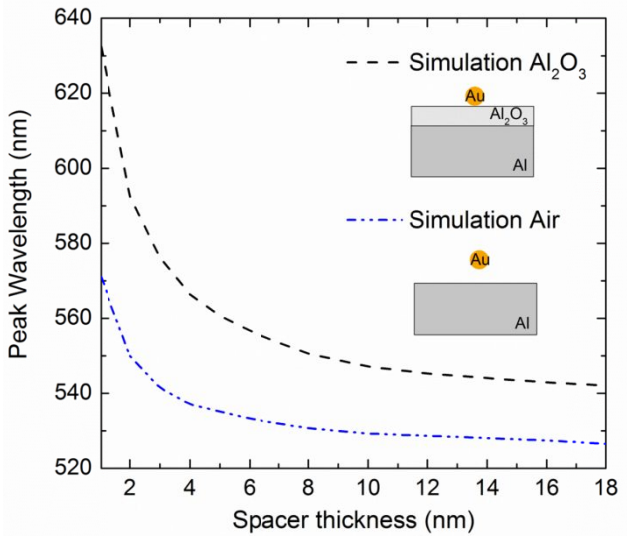

Figure 6. Gold nanoparticle scattering peak wavelength obtained using numerical simulations with either an Al_2O_3 film or an air gap as a spacer layer between the nanoparticle and the Al substrate.

5. CONCLUSION

The optical response of Au nanoparticles near an Al film was investigated. Dark-field microscopy images of single Au nanoparticles on Al_2O_3 coated Al films show ring-shaped scattering patterns, indicating z-polarized dipole oscillation. The thickness of the Al_2O_3 layer was varied through anodization. The color of the scattered light was seen to change gradually from orange to green as the thickness of the aluminum oxide layer was increased. Single particle spectroscopy on the same set of gold nanoparticles showed a gradual shift of the peak scattering wavelength, as well as some particle-to-particle variations. The observed trends in peak scattering wavelength of the single Au particles were reproduced in numerical calculations. The observed blue-shift of the peak wavelengths is attributed to a reduced coupling between the gold nanoparticle dipole moment and the dynamic image dipole formed by the nearby aluminum film. The effect of particle size variation was examined numerically at 4 nm oxide thickness, showing a red-shift as the particle diameter increases. The study demonstrates a way to tune the plasmon resonance wavelength of metal nanoparticles through a controlled chemical process, providing post-fabrication modification of the optical response of metal nanoantennas. This process could be useful as a resonance optimization technique for plasmon based optical sensing.

REFERENCES

[1] Camden, J. P.; Dieringer, J. A.; Zhao, J.; Van Duyne, R. P., "Controlled Plasmonic Nanostructures for Surface-Enhanced Spectroscopy and Sensing," Accounts Chem Res 41(12), 1653-1661 (2008).

[2] Li, J. F.; Huang, Y. F.; Ding, Y.; Yang, Z. L.; Li, S. B.; Zhou, X. S.; Fan, F. R.; Zhang, W.; Zhou, Z. Y.; Wu, D. Y., *et al.*, "Shell-isolated nanoparticle-enhanced Raman spectroscopy," Nature 464(7287), 392-395 (2010).

[3] Kleinman, S. L.; Ringe, E.; Valley, N.; Wustholz, K. L.; Phillips, E.; Scheidt, K. A.; Schatz, G. C.; Van Duyne, R. P., "Single-Molecule Surface-Enhanced Raman Spectroscopy of Crystal Violet Isotopologues: Theory and Experiment," J Am Chem Soc 133(11), 4115-4122 (2011).

[4] Chu, L. Q.; Forch, R.; Knoll, W., "Surface-plasmon-enhanced fluorescence spectroscopy for DNA detection using fluorescently labeled PNA as "DNA indicator"," Angew Chem Int Edit 46(26), 4944-4947 (2007).

[5] Guerrero, A. R.; Aroca, R. F., "Surface-Enhanced Fluorescence with Shell-Isolated Nanoparticles (SHINEF)," Angew Chem Int Edit 50(3), 665-668 (2011).

[6] Russell, K. J.; Liu, T.-L.; Cui, S.; Hu, E. L., "Large spontaneous emission enhancement in plasmonic nanocavities," Nat Photon advance online publication((2012).

[7] Moran, A. M.; Sung, J. H.; Hicks, E. M.; Van Duyne, R. P.; Spears, K. G., "Second Harmonic Excitation Spectroscopy of Silver Nanoparticle Arrays," J Phys Chem B 109(10), 4501-4506 (2005).

[8] Pu, Y.; Grange, R.; Hsieh, C. L.; Psaltis, D., "Nonlinear Optical Properties of Core-Shell Nanocavities for Enhanced Second-Harmonic Generation," Phys Rev Lett 104(20), (2010).

[9] Toroghi, S.; Kik, P. G., "Cascaded Plasmonic Metamaterials for Phase-Controlled Enhancement of Nonlinear Absorption and Refraction," Phys Rev B 85(4), 045432 (2012).

[10] Sathyavathi, R.; Krishna, M. B.; Rao, S. V.; Saritha, R.; Rao, D. N., "Biosynthesis of Silver Nanoparticles Using Coriandrum Sativum Leaf Extract and Their Application in Nonlinear Optics," Adv Sci Lett 3(2), 138-143 (2010).

[11] Liu, N.; Tang, M. L.; Hentschel, M.; Giessen, H.; Alivisatos, A. P., "Nanoantenna-enhanced gas sensing in a single tailored nanofocus," Nat Mater 10(8), 631-636 (2011).

[12] Huang, C. J.; Ye, J.; Wang, S.; Stakenborg, T.; Lagae, L., "Gold nanoring as a sensitive plasmonic biosensor for on-chip DNA detection," Appl Phys Lett 100(17), (2012).

[13] Atwater, H. A.; Polman, A., "Plasmonics for improved photovoltaic devices," Nat Mater 9(3), 205-213 (2010).

[14] Chen, X.; Jia, B. H.; Saha, J. K.; Cai, B. Y.; Stokes, N.; Qiao, Q.; Wang, Y. Q.; Shi, Z. R.; Gu, M., "Broadband Enhancement in Thin-Film Amorphous Silicon Solar Cells Enabled by Nucleated Silver Nanoparticles," Nano Lett 12(5), 2187-2192 (2012).

[15] Wu, J.; Mangham, S. C.; Reddy, V. R.; Manasreh, M. O.; Weaver, B. D., "Surface plasmon enhanced intermediate band based quantum dots solar cell," Sol Energ Mat Sol C 102(0), 44-49 (2012).

[16] Zhang, S.; Genov, D. A.; Wang, Y.; Liu, M.; Zhang, X., "Plasmon-induced transparency in metamaterials," Phys Rev Lett 101(4), (2008).

[17] Li, Z. Y.; Ma, Y. F.; Huang, R.; Singh, R. J.; Gu, J. Q.; Tian, Z.; Han, J. G.; Zhang, W. L., "Manipulating the plasmon-induced transparency in terahertz metamaterials," Opt Express 19(9), 8912-8919 (2011).

[18] Noguez, C., "Surface Plasmons on Metal Nanoparticles: The Influence of Shpae and Physical Environment," J Phys Chem C 111(10), 3806-3819 (2007).
[19] McFarland, A. D.; Young, M. A.; Dieringer, J. A.; Van Duyne, R. P., "Wavelength-scanned surface-enhanced Raman excitation spectroscopy," J Phys Chem B 109(22), 11279-11285 (2005).
[20] Dieringer, J. A.; Wustholz, K. L.; Masiello, D. J.; Camden, J. P.; Kleinman, S. L.; Schatz, G. C.; Van Duyne, R. P., "Surface-Enhanced Raman Excitation Spectroscopy of a Single Rhodamine 6G Molecule," J Am Chem Soc 131(2), 849-854 (2009).
[21] Oldenburg, S. J.; Jackson, J. B.; Westcott, S. L.; Halas, N. J., "Infrared extinction properties of gold nanoshells," Appl Phys Lett 75(19), 2897-2899 (1999).
[22] Haynes, C. L.; Van Duyne, R. P., "Nanosphere lithography: A versatile nanofabrication tool for studies of size-dependent nanoparticle optics," J Phys Chem B 105(24), 5599-5611 (2001).
[23] Sherry, L. J.; Chang, S. H.; Schatz, G. C.; Van Duyne, R. P.; Wiley, B. J.; Xia, Y. N., "Localized surface plasmon resonance spectroscopy of single silver nanocubes," Nano Lett 5(10), 2034-2038 (2005).
[24] Nordlander, P.; Oubre, C.; Prodan, E.; Li, K.; Stockman, M. I., "Plasmon hybridizaton in nanoparticle dimers," Nano Lett 4(5), 899-903 (2004).
[25] Willingham, B.; Brandl, D. W.; Nordlander, P., "Plasmon hybridization in nanorod dimers," Appl Phys B-Lasers O 93(1), 209-216 (2008).
[26] Mock, J. J.; Hill, R. T.; Degiron, A.; Zauscher, S.; Chilkoti, A.; Smith, D. R., "Distance-Dependent Plasmon Resonant Coupling between a Gold Nanoparticle and Gold Film," Nano Lett 8(8), 2245-2252 (2008).
[27] Knight, M. W.; Wu, Y. P.; Lassiter, J. B.; Nordlander, P.; Halas, N. J., "Substrates Matter: Influence of an Adjacent Dielectric on an Individual Plasmonic Nanoparticle," Nano Lett 9(5), 2188-2192 (2009).
[28] Diggle, J. W.; Downie, T. C.; Goulding, C. W., "Anodic Oxide Films on Aluminum," Chem Rev 69(3), 365-405 (1969).
[29] Hutchins, G. A.; Chen, C. T., "The Amorphous to Crystalline Transformation of Anodic Aluminum-Oxide during Anodization in an Ammonium Citrate Electrolyte," J Electrochem Soc 133(7), 1332-1337 (1986).
[30] Palik, E. D.; Ghosh, G., [Handbook of Optical Constants of Solids], Academic Press, Orlando; London, (1985).
[31] Lichtenstein, T., [Handbook of Thin Film Materials], Rochester, New York, (1979).
[32] CST MICROWAVE STUDIO®, Computer Simulation Technology, Darmstadt, Germany, (2011).
[33] Johnson, P. B.; Christy, R. W., "Optical Constants of the Noble Metals," Phys Rev B 6(12), 4370-4379 (1972).
[34] Jackson, J. D., [Classical Electrodynamics], Wiley, New York, (1962).